# Operando Electron Microscopy Study of Cobalt-Based Fischer-Tropsch Nanocatalysts

Kassiogé Dembélé, Mounib Bahri, Charles Hirlimann, Simona Moldovan, Adrien Berliet, Sylvie Maury, Anne-sophie Gay, Ovidiu Ersen

# *Operando* electron microscopy study of cobalt-based Fischer-Tropsch nanocatalysts

Kassiogé Dembélé[1,2], Mounib Bahri[1], Charles Hirlimann[1], Simona Moldovan[1], Adrien Berliet[2], Sylvie Maury[2], Anne-Sophie Gay[2], Ovidiu Ersen[1,3]*

[1] *Institut de Physique et Chimie des Matériaux de Strasbourg (IPCMS), UMR 7504 CNRS - Université de Strasbourg, 23 rue du Læss, BP 43, 67034 Strasbourg cedex 2 (France)*

[2] *IFP Énergies Nouvelles, Rond-point de l'échangeur de Solaize, 69360 (France)*

[3] *Institut Universitaire de France (IUF), 1 Rue Descartes Paris, 75231 (France)*

Dr. Kassiogé Dembélé, Dr. Mounib Bahri, Dr. Charles Hirlimann, Dr. Simona Moldovan, Adrien Berliet, Dr. Sylvie Maury, Dr. Anne-Sophie Gay, Prof. Dr. Ovidiu Ersen

*corresponding author: ovidiu.ersen@ipcms.unistra.fr

## Abstract

Thanks to their stability and selectivity for long-chains hydrocarbons, supported Co nanoparticles are the most commonly used catalysts in the Fischer-Tropsch synthesis reaction. We report here on the use of in situ transmission electron microscopy (TEM) to address the real-time evolution of cobalt-based catalysts during their reduction under relevant industrial activation condition ($10^5$ Pa, 430°C), and their operation in syngas ($H_2$/CO=2, $10^5$ Pa, 220°C). To do so, we chose $Co_3O_4$-Pt nanoparticles supported on silica or alumina that can be directly compared to some industrial catalysts. By analysing the real space information contained in the TEM images, we have monitored the fragmentation of cobalt aggregates, the disappearance of cavities within the particles, their shape changes, the particle diffusion and coalescence processes, as well as the effect of the support (silica or alumina) on the behaviour of the Co phase. An easier reduction of cobalt catalysts supported on silica as compared to the same catalyst supported on alumina was also observed. During the catalyst operation under syngas, we have noticed the stability of the general shape of the particles. Simultaneously, using a residual gas analyser connected to the TEM holder, the main gas products of the Fischer-Tropsch reaction were systematically analysed. Our findings underline the benefit of the *operando* TEM to study the dynamical evolution of catalysts, at the nanoparticle level, under operation conditions.

**Keywords**: *in situ* TEM, cobalt-based catalysts, reduction, syngas conversion, Fischer-Tropsch synthesis, *operando* study.

## Introduction

The Fischer-Tropsch synthesis (FTS) produces hydrocarbons from the hydrogenation of carbon monoxide.[1–4] For this reaction, different metallic particles can be used as the active catalyst phases: Fe, Co, Ni, Ru...[2,5–7] However, due to their selectivity for long-chains hydrocarbons and to their stability, supported cobalt particles are the most common catalysts employed in industry for producing synthetic fuel.[3,8] To disperse and stabilize these metallic particles, metal oxides such as alumina, silica or titania are generally used as supports.[9,10] The nature of the oxide support plays an important role on the cobalt particles dispersion, on their reducibility and therefore on their catalytic performance.[11–13] In addition, in order to improve the catalyst reduction and its dispersion on the support, noble metals such as Ru and Pt can be used as promoters.[14]

Most commonly, cobalt catalysts are prepared by incipient wetness impregnation of a cobalt precursor on the support. After drying and eliminating the residue of the cobalt precursor through calcination, one gets cobalt oxide particles generally as supported $Co_3O_4$ that needs to be reduced in order to obtain the metallic particles, which are the active phase for the FTS reaction.[3,15] This activation step is ideally achieved by heating the catalyst under exposure to dihydrogen or carbon monoxide gases at atmospheric pressure.

Various characterization methods able to provide averaged information on the catalyst, such as X-Ray Diffraction (XRD) or temperature programmed reduction (TPR), have been systematically used to assess the properties of the as-synthesized catalysts, as well as their structural modifications during their activation step or operation under FTS conditions.[16,17] For instance, using a homemade high-pressure cell and combining X-ray Absorption Spectroscopy (XAS) and XRD techniques, Loewert et al.[16] have monitored the changes in Co-Ni-Re/$\gamma Al_2O_3$ catalysts during activation ($H_2$, 1 bar, and 450°C), and the subsequent FTS ($H_2$/CO, 250 °C and 30 bar). They observed that the catalyst activation starts at 260 °C with $Co_3O_4$ reduction into CoO followed by the $Co^0$ formation at 340 °C. Afterwards, during the first hours of the FTS process, they provided direct evidence of the presence of a liquid-like carbon film around the catalyst which hinders the mass transport and therefore CO conversion. Finally, at longer reaction time, the catalyst undergoes subsequent deactivation due to the formation of a cobalt aluminate phase and of some various carbon species (amorphous carbon, carbide, graphite…). From a general point of view, such a global study allows thus to obtain very useful information on the catalyst evolution and the

involved phenomena. However, one of the major drawbacks of such global approaches is that the obtained information is averaged over the whole catalyst and cannot be spatially solved at the particle level with a nanometre resolution, in order to be able to distinguish, for example, the behaviour of isolated particles from that of aggregates or to obtain local information as a function of the particle localisation with respect to the support.

In this framework, transmission electron microscopy, especially when used in the *in situ* mode, may provide valuable and complementary insight on the morphology and structure of individual particles during their activation.[18–23] Ward et al.[24] have investigated non-supported cobalt oxide particles reduction under $H_2$ gas using environmental TEM (ETEM). They showed that the $Co_3O_4$ particles reduction into CoO starts at a temperature of 200 °C and a pressure of 10 Pa. In the case of particles larger than ~15 nm, the reduction process leads to the formation of an interface between the initial $Co_3O_4$ and the formed CoO phase in the particle. While the reduction is ongoing, a topotactic growth does occur in which the interface penetrates deeper inside the particle. However, only CoO particles were observed at temperatures up to 400 °C and no metallic $Co^o$ could be detected at 10 Pa. At higher temperature (450 °C) and higher pressure (300 Pa), the authors observed partial reduction of some particles into metallic fcc Co, and they finally suggested that higher pressures and temperature are required to fully reduce the particles into $Co^0$.

In the case of supported catalysts, the presence of the support does increase the reduction temperature by 30°C - 50°C as reported by Paryjczak et al.[25] Using alumina-supported cobalt particles in an ETEM, Dehghan et al. reported similar results for $Co_3O_4$ particles reduction into CoO starting at 180 °C and 340 Pa.[26] Using high-resolution TEM (HRTEM) and electron energy loss spectroscopy (EELS), the authors also detected the particles reduction at 360 °C with the presence of both hcp and fcc metallic cobalt phases. However, only a partial reduction of the particles could be observed due to the limited pressure of 340 Pa. In addition, it has been shown that the particles could undergo re-oxidation when cooling the catalyst down to the room temperature even under $H_2$ exposure, due to the presence of residual water vapour in the vacuum system of the ETEM. Therefore, a more relevant activation study requires investigating the individual particles evolution under a reducing gas at higher pressures, in order to get closer to reduction conditions used in industrial processes. In addition, to be able to directly transpose the information obtained by environmental TEM to the understanding of the material behaviour in the

real catalytic reactors, the *in situ* studies should be performed on industrially relevant catalysts, having similar structures and 3D architectures.

In this context, we report here on the real-time evolution of industrial-like cobalt-based catalysts during their reduction under relevant activation conditions ($10^5$ Pa, from room temperature to 430 °C) and their operation in FTS reactions at atmospheric pressure, using *operando* TEM. With the catalyst in a TEM environmental sealed cell and the benefits of the high angle annular dark field (HAADF) mode in scanning TEM (STEM) in terms of resolution and contrast, our goal was to monitor the structural changes at the individual particle level with nanometric resolution. In a first step, we investigated the typical morphological changes that do occur on a platinum promoted cobalt oxide-based catalyst and developed a methodology to rationalize the observation of the evolution under reducing atmosphere. Such direct information then allows evaluating the role of the support nature during the activation by comparing silica and alumina supported cobalt. In a second step, we monitored the catalyst behaviour when exposed to syngas ($CO/H_2$) flows at atmospheric pressure during a time duration compatible with *in situ* TEM analysis. In addition, the last goal was to measure in real time the gases produced during the syngas exposure using a mass spectrometer connected to the exhaust line of the *gas cell* TEM holder. It should be mentioned that this is one of the few *in situ* TEM experiments[27,28] reported in the literature until now providing results obtained on industrial-like catalysts when using a gas-cell TEM holder combined with a mass spectrometer. Note that, in a previous paper, we already reported on the in situ study of such a supported catalytic system; however the main goal of that work was to monitor the thermal behavior of cobalt nanoparticles in various types of gases and, in addition, the experimental conditions we used are not relevant for the catalyst activation and FT synthesis.[29]

## Materials and methods

**Catalyst preparation.** The catalysts were prepared via incipient wetness impregnation using aqueous solutions of cobalt nitrate [$Co(NO_3)_2, 6H_2O$] on three different commercial supports: silica-doped alumina (95% $Al_2O_3$ - 5% $SiO_2$); alumina (Sasol, Puralox®) and silica (Grace Davisil 634). The target concentration for all catalysts was 14% wt cobalt. To get similar textural properties for alumina and silica support, commercial silica gel was first calcined at 900 °C for 4 h in order to decrease its specific surface area. Platinum was used as a promoter in order to facilitate the activation of the catalyst.

***Catalyst for the development of the operando methodology.*** To first develop the *in situ* and *operando* methodologies, we have used an industrial catalyst that presents a high activity and reducibility. This catalyst was prepared on the high porous volume silica-doped alumina support using a simplified protocol. This catalyst was prepared by co-impregnating in one step 13% wt cobalt and 100 ppm platinum. The platinum addition was achieved by using a tetra-amine platinum hydroxide aqueous solution containing 9% platinum. After a 90 min maturation period, it was dried in a tubular reactor under flowing air at 80 °C during 5 h, then it was calcined in the same reactor at 360 °C for 4 h after a temperature increase ramp of 1°C/min under 1 Nl/h/g solid. These conditions do favour the formation of large cobalt oxide particles.

***Catalysts for the assessment of the support effect.*** Two successive impregnation steps were necessary to obtain the desired cobalt amount for silica and alumina supports. Platinum was co-impregnated using the tetra-amine platinum hydroxide aqueous solution with cobalt nitrate during the second impregnation step. A large amount of platinum was used in order to facilitate the activation study. In order to improve the cobalt dispersion for the two catalysts and to narrow the particle size distribution, ethylene glycol was added to the impregnating solution for each impregnation step.[11] The amount of ethylene glycol (EG) was chosen in order to obtain small cobalt particles, with a ratio $R=mH_2O/(mH_2O+mEG)$ equal to 0.8. After impregnation, a maturation period of 90 min was respected, allowing for the capillary migration of the cobalt precursor inside the pores. The maturation step was followed by an oven drying period under pulsed air at 85 °C for one night and calcination at 420 °C for 4 h. The grains size and cobalt repartition inside the grains were analysed using a Zeiss supra 40 scanning electron microscope; the BET surfaces areas were determined by nitrogen physisorption at 77 °K using an ASAP 2420 instrument; the average $Co_3O_4$ crystallites sizes were determined using XRD and the Scherrer equation, on a PANanalytical diffractometer; and the cobalt loading was obtained through X-Ray Fluorescence (XRF) using a Thermo Advant'X system. The obtained physicochemical characteristics of the three catalysts after their preparation are presented in Table 1. Overall platinum contents were respectively determined by inductive coupling plasma (ICP) measurement.

**Temperature Programmed Reduction (TPR).** The reducibility of the catalysts was determined by means of temperature programmed reduction. TPR analysis was carried out on an AutoChem II 2920 V4.03 apparatus from Micromeritics®. About 0.5 g of catalyst was exposed to 58 NmL/min of $5\%H_2$/Ar while heating from room temperature to 1000 °C with a 5 °C/min ramp.

***Operando* TEM investigations**. The powders of the catalysts precursors were crushed, then dispersed into pure ethanol and drop-casted onto the *in situ* cell membrane of a Protochips Atmosphere holder. In this holder, two microelectromechanical system (MEMS) chips (2 mm x 2 mm for the small chips and 4.5 mm x 6 mm for the large chips) are mounted as closed-cell with the gas confined between them, into a thickness of 5 µm. The chips consist of small SiNx windows (90 x 90 $\mu m^2$ for the heated chip and 300 x 300 $\mu m^2$ for the sealing chip) which are transparent to the electron-beam. In the main chip, on which we deposit the sample, the SiNx membrane is in contact with a heating-ceramic SiC film. This later contains 6 holes with a diameter of 10 µm for facilitate the sample observation in the TEM, and is heated by applying an electrical current through gold contacts. Thereby, it is possible to heat the sample up to 1000 °C with a temperature rate of 5 °C/s. Due to the small size of the heating area (90 x 90 $\mu m^2$), a homogenous temperature distribution is obtained within the analysed areas, with a precision of ±3°C. Additional details regarding the geometry and the mounting of the gas cell are given in Figure SI-1.

Due to the small dimension of the chips and the ethanol evaporation after samples deposition into the main chip, it was not possible to precisely weight our samples. However, in order to be able to compare the three catalysts, we have prepared similar concentration (1.6 mL/g) and the same amount of the sample was set onto the chip for each experiment. Hence, we have deposited three droplets of 1 µL, from which we could assume a chip contains ideally 1 µg after ethanol evaporation.

In order to obtain the highest possible contrast between the particles and the supports, the scanning TEM with high angle-annular dark field (HAADF) imaging mode was performed, using a Cs aberration corrected JEOL (2100F) microscope, which was operated at 200 kV. To avoid the sample damage by the electron beam, the electron dose rate was kept below $10^5$ e $nm^{-2}$ $s^{-1}$, and additional areas – not previously exposed to the beam– were systematically observed for comparison to demonstrate that the observed areas were not damaged. All the supported cobalt oxides were studied at atmospheric pressure using the following procedure: i) initial observation under neutral Ar atmosphere at 200 °C; ii) activation under a $H_2$ flow from 200 °C to 430 °C with a heating ramp of 5 °C/min which is maintained for 30 min, then decreased to 220 °C and iii) exposure to the $H_2$/CO (2:1) mixture at 220 °C for 1 h. For all the experiments, a flow-rate of 0.08 mL/min was used. For minimizing the effect of the electron beam on the catalysts during data acquisition, the beam was switched off during the changes of the type of gas. In addition, in order

to analyse the gas reactants and products, the exhaust line of the holder was connected to a residual gas analyser (RGA) from the Protochips company.[30] This later combines a differential pumping system with a quadrupole mass analyser (QMA 200). The gas products were analysed through electron ionization using multiple ion detection (MID) acquisition from the QUADERA software (Pfeiffer-vacuum). The gas products were subsequently analysed by considering their main mass to charge (m/z) ratio, which can be obtained from the NIST database. Finally, the ionic currents of the individual products were normalized to the one of the carbon monoxide reactant.

**Catalytic tests.** Catalysts performances were determined on a High Throughput Experimentation (HTE) unit from the Avantium company. The unit is equipped with sixteen parallel fixed bed reactors (2 mm ID), with a common feed-gas equally distributed between each reactor. Pressure is regulated for each reactor independently, and is based on the values measured at the entrance of the reactors. Four heating blocks are used to control reactors temperature by group of four, and temperatures are measured in three different zones of the heating blocks to ensure temperature homogeneity inside the catalytic beds. Products and unreacted reactants are collected downstream. Heavier products are separated from light ones by a cold trap (80 °C). Light products are analysed on-line up to $C_{10}$ hydrocarbons by gas chromatography and heavy products can be analysed off-line by simulated distillation analysis. Helium is used as an internal standard for gas flow calculation and is analysed by a TCD detector, along with $N_2$, CO, and $H_2$, which are separated through a molecular sieve column. The lightest hydrocarbons cut ($C_1$–$C_8$) are separated from the heavy hydrocarbons one ($C_9$–$C_{14}$) by a first HP-INNOwax column. The light hydrocarbons are then separated using a GS-GasPro column while the heavy ones using a second HP-INNOwax column. The total outlet flowrate Q_out, the flowrates Q_(i,out) specific to the various compounds and the conversion and selectivity parameters are calculated according to the formula given in SI. For the tests, 200 mg of each oxide catalysts were loaded and then reduced *in situ* under 0.45 $NL \cdot h^{-1}$ of pure hydrogen at 400 °C during 16 h after a ramp of 2 °C/min from ambient temperature to 400 °C. After reduction, temperature was decreased to 180 °C under hydrogen and the pressure progressively raised to 20 barg. Syngas was finally injected with a flow-rate of 4.6 Nml/min containing 5% He and temperature increased to 210 °C (following a ramp of 1 $°C \cdot min^{-1}$). The CO flow-rate was varied between 1.9 and 4.6 Nml/min in each reactor in order to obtain different conversion levels and plot the conversion/$C_{5+}$ selectivity curve. The inlet $H_2$/CO ratio was always adjusted to 2.12.

## Results and discussion

**Physicochemical characteristics of the catalysts.** Table 1 presents the obtained physicochemical characteristics of the three raw catalysts. The two catalysts with silica-doped alumina and alumina supports present similar grains size and BET surface area. On the other hand, compared to the catalysts supported on pure alumina and silica, the catalyst supported on silica-doped alumina presents a slightly higher cobalt content as well as a larger pore size, which favours the formation of bigger $Co_3O_4$ crystallites. In addition, for the alumina and silica supports, the presence of EG in the impregnation solution allowed for a better dispersion of the cobalt and led to smaller $Co_3O_4$ crystallites size. It is commonly described in the literature that small particles (< 6 nm) favours the activity for FTS and the selectivity towards methane, whereas it limits the formation of $C_{5+}$ products.[31,32] Considering the standard deviation on the platinum and cobalt content measurements, it can be considered that the catalysts on silica and alumina do contain similar metal amounts. It is also worth noting that their Pt amounts is higher than in the case of the catalyst on silica-doped alumina, as the latter was chosen to be similar to an industrial one and, therefore, the Pt amount should be limited due to its high cost.

Table 1. Physicochemical characteristics of the as prepared cobalt-based catalysts.

| | | Support properties | | | | Catalyst properties | | |
|---|---|---|---|---|---|---|---|---|
| | | Grains size (µm) | BET surface (m2/g) | Porous volume (cm3/g) | Pores diameter (nm) | Cobalt loading (% wt.) | XRD mean Co3O4 crystallite size (nm) | Platinum content (ppm) |
| Silica-doped alumina | | 80 | 170 | 0.84 | 20 | 15.0 ± 3 | 16 ± 3 | 100 ± 10 |
| Alumina PURALOX | | 80 | 166 | 0.44 | 10.8 | 13.3 ± 3 | 6 ± 0.5 | 355 ± 35 |
| DAVISIL® silica gel Grade 634 | before treatment | 75-150 | 460 | 0.75 | 5.9 | - | - | |
| | after treatment | 50-100 | 247 | 0.36 | 6 | 12.4 ± 3 | 7 ± 0.5 | 280 ± 28 |

First information on the catalyst behaviour during the reduction process was obtained by TPR. The corresponding TPR profiles are shown in Figure SI-2. Several peaks of reduction can be observed

and assigned to the reduction of different cobalt species. The first main hydrogen consumption region can be attributed to the reduction of $Co_3O_4$ into CoO (in a range between 200 and 380 °C) while the second region (ranging from 380 to 650 °C) can be unambiguously assigned to the transformation of CoO into metallic cobalt. The hydrogen consumption above 650 °C originates from the reduction of the species constituting either small cobalt particles in strong interaction with the support or cobalt aluminate for the Co-Pt/$Al_2O_3$ catalyst or silicate for the Co-Pt/$SiO_2$ one. The rather wide reduction area for each Co species can be due to the presence of cobalt particles of different sizes, the smallest particles being reduced at higher temperature. The profiles are significantly different for the two studied catalysts and do illustrate the highest reducibility of cobalt over silica as its reduction occurs at lower temperature.

From a microstructural point of view, is it worth to note that, although Co-Pt/$Al_2O_3$ catalyst consists of irregular round grains with sizes from 15 to 150 µm whereas Co-Pt/$SiO_2$ presents rather faceted grains with diameters between 15 and 1200 µm. However, in both catalysts, Co is quite homogeneously dispersed in the form of aggregates below dozens of nm, with very few local over-concentrations and some bigger aggregates (Figure SI-3).

**Catalytic properties.** The CO conversion as a function of time on stream and carbon monoxide flow rate is shown on Figure SI-4 for both catalysts supported on pure alumina and pure silica. The initial conversion is higher on cobalt over silica catalyst (about 33% more) than on cobalt on alumina one. The cobalt particle size being similar, the difference is most probably due to the higher reduction degree of cobalt on silica because of lower interactions between support and cobalt oxide which facilitates the reduction process. Indeed, although the reduction rate cannot be determined before the catalytic testing on THE unit, *ex situ* reduction studies and magnetic measurements gave a reduction rate of 60% for Co-Pt/$Al_2O_3$ and of 77% for Co-Pt/$SiO_2$. On the other hand, the deactivation is also more pronounced as it can be observed after 15 h of time on stream (see tendency curves between 4 and 24 h), when the CO flow rate was the same as initially and the conversion on silica catalyst decreased by 20% whereas alumina catalyst has lost only 2% compared to the initial conversion. After 50 h time on stream; both catalysts show comparable CO conversions. This can be due to two independent reasons: first, the cobalt on silica catalyst is more prone to sintering because its interaction with the support is weaker compared to cobalt on alumina; second, the higher conversions obtained for the first catalyst do accelerate the deactivation via the particle sintering and/or oxidation which can be currently observed in Fischer-Tropsch conditions

in the case of small particles in a water rich environment. Finally, regarding the selectivity, as shown in Figure SI-5, both catalysts present similar $C_{5+}$ selectivity dependences on the CO conversion.

At this stage of the study, to better understand the difference between the behaviour of the catalysts and to provide a clear and direct insight on the reduction and deactivation processes, a microstructural study, spatially solved at the particle level, is required. This is the goal of the *operando* TEM studies we will detail hereafter.

***Operando* TEM: activation step of Co-Pt/$Al_2O_3$-$SiO_2$**

Figure 1 shows typical *in situ* STEM-HAADF images of a representative area of the sample before (a) and after exposure to $H_2$ (b). Both isolated cobalt nanoparticles (NPs) and aggregates are initially observed on the $Al_2O_3$-$SiO_2$ support. The particle aggregates with size of 20 - 40 nm do exhibit an interconnected porous-like structure, whereas the support presents a rod-like structure due to $Al_2O_3$. It should be noted that, at this point, the images are fuzzy due to a weak contrast between the particles and the crystalline alumina support. Hence, it is not possible to precisely measure the cobalt particles size. Moreover, the presence of a small amount (few hundred of ppm) of Pt, which is distributed all over the cobalt-oxide particles and the support, cannot be observed in the STEM-HAADF image.

After $H_2$ exposure, a higher contrast is noticeable between the particles and the support. In addition, the particles aggregates do undergo fragmentation into individual particles (**Figure** 1a and b). These morphological changes are better emphasized by visualizing a combined image obtained by adding of colourized images before (in red) and after $H_2$ (in green) exposure as shown in **Figure** 1c. With the heating under $H_2$ exposure, the apparent particles surface decreases compared to the pristine catalyst. By assuming a spherical shape for the isolated particles, a mean size of 8.9 ± 2.5 nm was measured (**Figure** 1d).

The simultaneous increase of the contrast between the cobalt particles and the support and the decrease of the apparent particle surface area is clearly an indication of the particles densification, which is a result of oxygen removal during the cobalt reduction and the related crystal lattice contraction (expected to be close to 0.8). The morphological changes corresponding to the particles aggregates fragmentation and densification are in line with previous *ex situ* TEM studies on Co-Re/$TiO_2$ reduction at higher pressure (1.2 MPa).[33,34] It should be noted that the particle size is smaller than expected when considering the average particle size determined by XRD and the

particle size decreases by 20 % (12 nm) after reduction. This discrepancy may occur as we did not consider the particle aggregates for the size measurement, and the XRD measurement is more sensitive to larger particles/aggregates size. It should also be noticed that the particle aggregates fragmentation is beneficial for the catalyst as it favours the cobalt dispersion, therefore enhancing the number of active sites available for the syngas conversion.

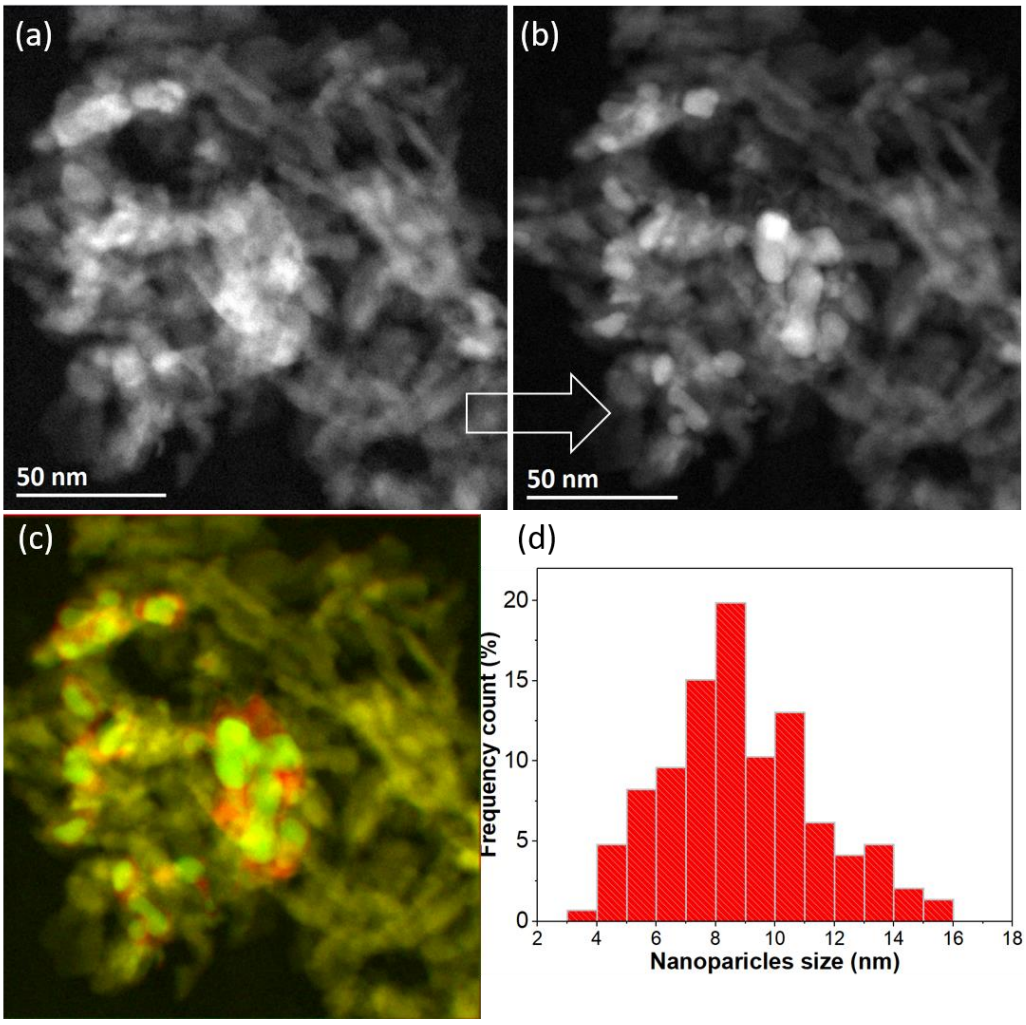


**Figure 1.** *In situ* HAADF-STEM images of the $Co_3O_4$-Pt/$Al_2O_3$-$SiO_2$ catalyst initially observed under Ar (a) at 200 °C, and 101.3 kPa; then exposed to $H_2$ (b) at 430 °C, and 101.3 kPa. (c) is the addition of the coloured images (a) in red and (b) in green. Particle size distribution under $H_2$ exposure at 430 °C (d).

In order to better understand the reduction process, we have followed the morphological changes during the temperature increase from 200 °C to 430 °C under $H_2$. **Figure 2** depicts a representative area of the catalyst initially observed under Ar and its evolutions under $H_2$ at different

temperatures. To increase the image contrast and underline the changes, we have filtered the STEM-HAADF images using a bandpass filter. Hence, the presence of cavities in the aggregated particles starts to be clearly visible at 287 °C (see dotted circles in **Figure 2**b). Then, particle formation from an aggregate occurred at 340 °C (see full circles in **Figure** 2c). At higher temperature, 380 °C (**Figure 2**d), a large amount of particle aggregates did fragment into individual particles. In addition, the contrast between the support and the individual particles increased suggesting a densification of the particles. Moreover, the particles morphology changed towards an elongated shape. The main morphological modifications appeared to be achieved at 400 °C (**Figure** 2e), except for the on-going particles diffusion and coalescence at 430 °C (**Figure** 2f). Regarding the structure of the activated catalyst, we have chosen to use STEM imaging conditions, which allows to minimize the total electron dose and the beam damages; for the same reason, no HRSTEM images were acquired. Thus, this does not allow to directly investigate the presence of hcp or fcc structures in the particles. Nevertheless, as the reduction of NPs and aggregates was conducted under pure hydrogen at 430 °C, the presence of hcp and fcc Co mixture is expected.[24,26]

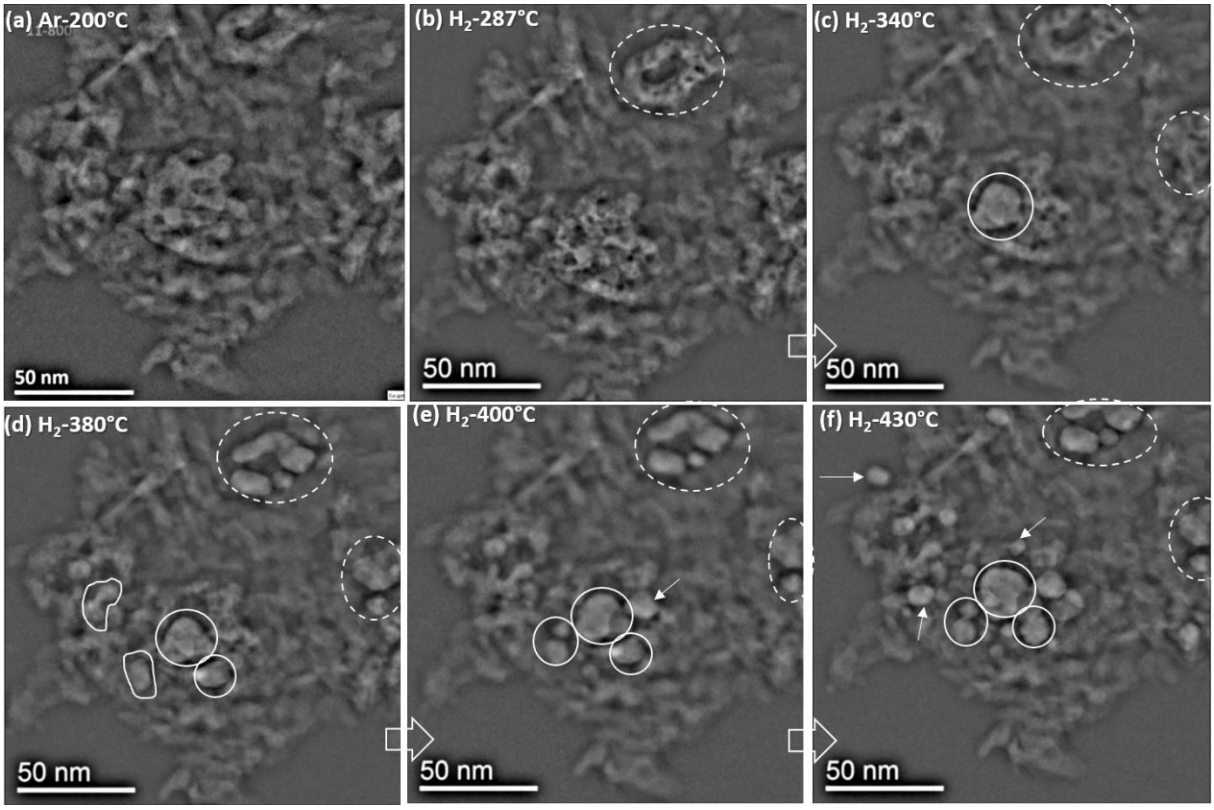


**Figure 2.** Band-pass filtered HAADF-STEM images of a representative area of $Co_3O_4$-Pt/$Al_2O_3$-$SiO_2$ catalyst initially observed under Ar (200 °C, 101.3 kPa) and its evolution during the temperature increase from 200 °C to 430 °C under $H_2$ at 101.3 kPa (b-d).

### *Operando* TEM: effect of the support on the catalyst activation

For similar particle sizes, the reduction is presumed to be easier using the silica support compared to the alumina one.[15,35] In order to understand the effect on the activation of the cobalt particles-support interaction, we investigated the Co-Pt/$Al_2O_3$ and Co-Pt/$SiO_2$ catalysts. **Figure** 3 shows representative *in situ* STEM-HAADF images of the Co-Pt/$SiO_2$ and Co-Pt/$Al_2O_3$ catalysts exposed first to Ar (200 °C, 101.3 kPa) then to $H_2$ (430 °C, 101.3 kPa). The contrast between the particles and the support is higher with silica (**Figure** 3a) as compared to alumina (**Figure** 3d). Thereby, the presence of cavities can be easily noticed inside some particles. Both Co-Pt/$SiO_2$ and Co-Pt/$Al_2O_3$ do present a high dispersion of the cobalt oxide particles on the support under the Ar exposure. Once again, we cannot precisely measure the initial cobalt oxide particles size since their apparent shape deviates from a spherical morphology and, in addition, a lower contrast characterizes the Co-Pt/$Al_2O_3$ catalyst. Then, in the Co-Pt/$SiO_2$ catalyst, particles fragmentation,

voids disappearance and morphological changes occurred with the temperature increased to 430 °C under $H_2$ (**Figure** 3b). However, the most significant change is the contrast increase between the particles and the support. Similar phenomena, suggesting the reduction of the catalyst, occurred in the Co-Pt/$Al_2O_3$ catalyst at 430 °C under $H_2$ (**Figure** 3e). Using the spherical-shape assumption for the particles, average sizes of 6.2 ± 2.3 nm and 5.0 ± 1.0 nm were respectively obtained for Co-Pt/$SiO_2$ and Co-Pt/$Al_2O_3$ after reduction at 430 °C

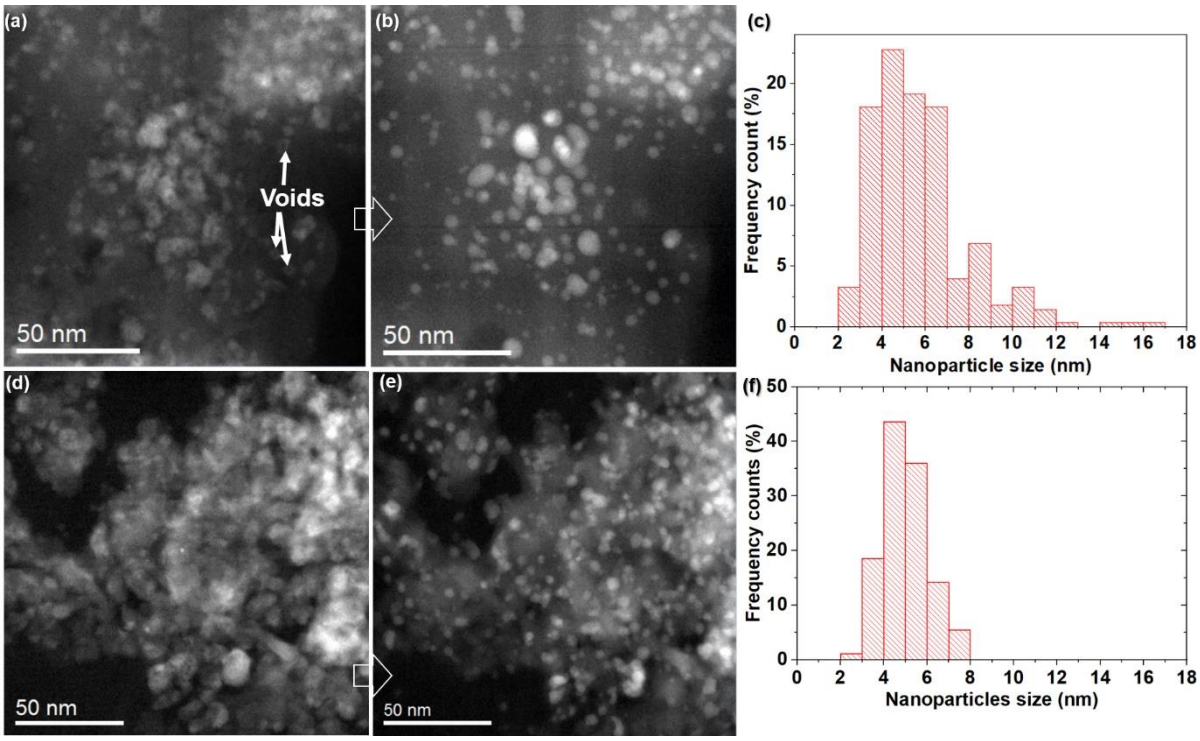


**Figure 3.** *In situ* STEM-HAADF images of representative areas of Co-Pt/$SiO_2$ (a-b) and Co-Pt/$Al_2O_3$ (d-e) observed under Ar (200 °C, 101.3 kPa) then under $H_2$ (430 °C, 101.3 kPa). Particle size distribution under $H_2$ exposure at 430 °C for Co-Pt/$Al_2O_3$ and Co-Pt/$SiO_2$ (c and f respectively).

Additional studies of the influence of silica and alumina supports on the activation step were conducted by following the individual particles morphology during the temperature increase under $H_2$ from 200 °C to 430 °C (**Figure 4**). In the case of Co-Pt/$SiO_2$ (**Figure 4**a-d), the loss of cavities within the particles and the formation of spherical particles started at 230 °C- 240 °C. Then, between 240 °C and 280 °C the particles fragmentation occurred in addition to the cavity's disappearance. Later, particles diffusion and coalescence were detected around ~ 280 °C-300 °C,

up to 430 °C. On the contrary, there was no apparent morphological change in the Co-Pt/$Al_2O_3$ before 270 °C. At 280 °C-300 °C (**Figure 4**f), particles fragmentation occurred. Thereafter, at 300-380 °C (**Figure 4**g), the disappearance of cavities inside the particles as well as the particles migration and coalescence (MC) were observed and continued until 430 °C (**Figure 4**h). The herein temperature delay, at which characteristic changes are observed, could be assigned to an easier reduction of the particles on a silica support compared to alumina. A similar behaviour was observed by TPR[35] and XRD[36] and was attributed to a weaker interaction between the cobalt particles and the silica support.

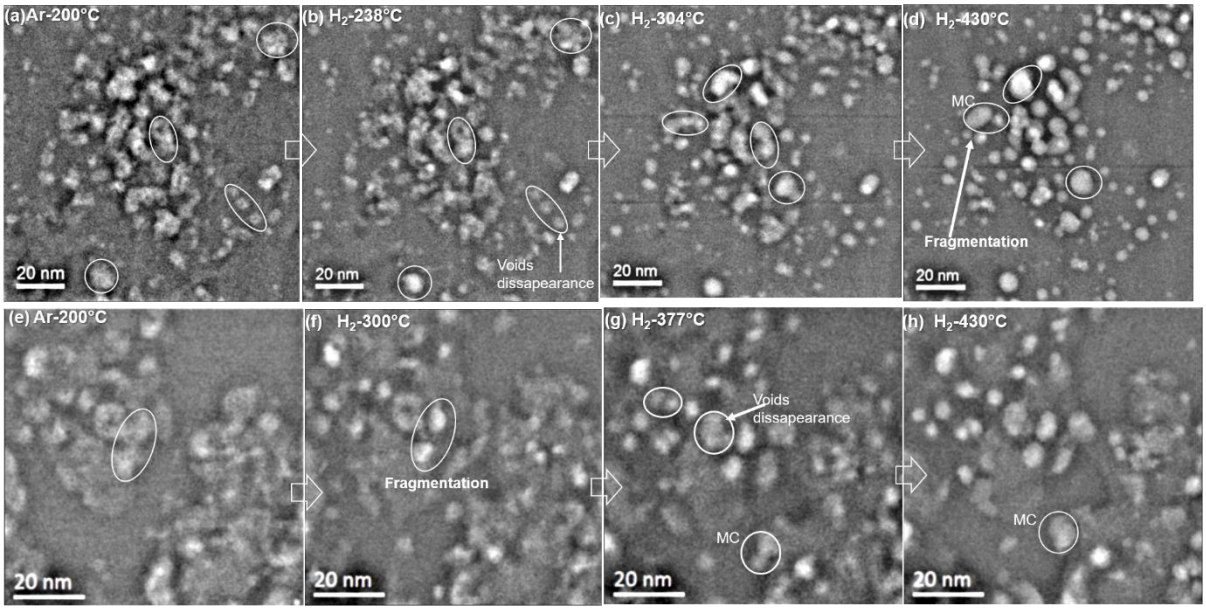


**Figure 4.** Bandpass filtered HAADF-STEM images of representative areas of $Co_3O_4$-Pt/$SiO_2$ (a-d) and $Co_3O_4$-Pt/$Al_2O_3$ (e-h) catalyst initially observed under Ar (200 °C, 101.3 kPa) and their evolution during the temperature increase from 200 °C to 430 °C under $H_2$ at 101.3 kPa.

### *Operando* TEM: catalysts behaviour under syngas ($H_2$/CO=2)

After activation, we have investigated the catalysts morphology and size evolution during their operation under 101.3 kPa of syngas mixture ($H_2$/CO=2) at 220 °C. As shown on **Figure 5**, the particles do present similar morphologies after activation and during syngas synthesis. However, we have observed slight changes that do correspond to particles migration and coalescence (**Figure 5**a-b) in the Co-Pt/$SiO_2$ catalyst. In addition, particles diffusion was observed on the Co-Pt/$Al_2O_3$ catalyst (**Figure 5**d-e). The average sizes of 7.1 ± 2.4 nm and 5.7 ± 1.0 nm were respectively

measured for Co-Pt/$SiO_2$ (**Figure 5**c) and Co-Pt/$Al_2O_3$ (**Figure 5**f) catalysts after syngas exposure. The cobalt particle size evolution observed here is negligible compared to previous studies on Co-Pt/$Al_2O_3$ catalyst reported by Moodley et al.[4,37,38] The authors have observed the sintering of the particles during the FTS reaction with a dominant Ostwald ripening and also particles migration and coalescence processes. This discrepancy is likely due to the limited pressure (101.3 kPa), shorter time on stream (1 h) and a likely lower conversion level used in our *in situ* TEM set-up compared to their studies achieved in slurry bubble column reactor at a higher pressure (2 MPa) and temperature (230 °C) at syngas conversion of 50-70 % for more than 400 h time on stream. Nonetheless, according to the literature, the best catalytic performances (high activity and selectivity) is expected for the optimum particles size of 6-8 nm at low pressure of 100-135 kPa.[31,39] Therefore, it can be assumed that particles size increase does not significantly alter the catalyst performance for FTS reactions.

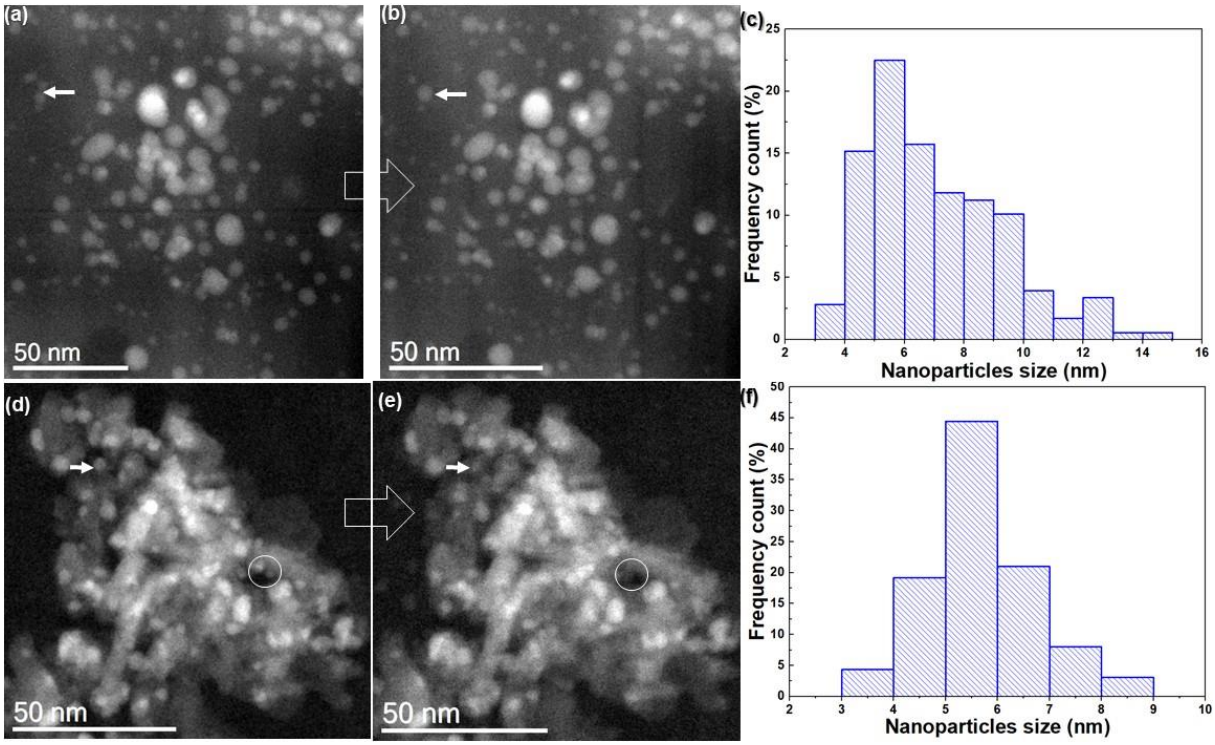


**Figure 5.** *In situ* STEM-HAADF images of representative areas of Co-Pt/$SiO_2$ (a-b) and Co-Pt/$Al_2O_3$ (d-e) observed under $H_2$ (430 °C, 101.3 kPa) then under syngas ($H_2$/CO=2, 220 °C, 101.3 kPa). Particle size distribution under $H_2$ exposure at 430 °C (c and f).

During the catalyst operation in the FTS reaction, the gas products (**Figure 6**) were quantified using the mass spectrometer. In both Co-Pt/$SiO_2$ (Figure 6a) and Co-Pt/$Al_2O_3$ (Figure **6**6b), we detected the presence of methane (m/z=15), $C_2$ (m/z=27 and 25), $C_3$ (m/z=26) and $C_{4+}$ (m/z=42 and 43). The ion currents of the individual m/z products were normalized to the initial one of the CO reactant. The results show relative small amounts of the reaction products, which may indicate a low CO conversion. This is likely due to a low amount of the sample into the gas cell and relatively low pressure of 101.3 kPa used for FTS reaction. An additional reason could be related to the geometry of the environmental cell: the heated area is relatively small (90 x 90 $\mu m^2$) compared to the total area of the chip encompassing by the sample. This implies that other areas of the sample, which were deposited far away from the SiNx may not be reduced and therefore may not contribute to the CO conversion. This hypothesis could be corroborated by the finding of van Ravenhorst et al.[22] Although these authors have used a different geometry in their microreactor, they have shown the presence of temperature heterogeneity on a resistive Pt-heater spiral with a 300 µm size. However, the ion currents signals do continue to increase during the time on stream at 220 °C, suggesting that the steady state is not reached after 1h under syngas. Consequently, it is not really possible to strictly compare the CO conversion for the two catalysts. Moreover, the exact mass of catalyst loaded in the TEM gas cell is quite difficult to measure, thus making a precise intrinsic activity comparison uneasy. Nevertheless, the ion currents normalization to the one of CO allows comparing the selectivity for different products formed during the time on stream. Hence, in both Co-Pt/$SiO_2$ and Co-Pt/$Al_2O_3$ catalysts, the following increasing order of selectivity could be established: $C_{4+} < C_3 < C_2 <$ methane. The methane appears as the main reaction product detected. This result can be explained by the limited pressure (atmospheric) we use in the environmental cell. This relatively low atmospheric pressure is known to favour methanation rather than hydrocarbon chain-growth.[3,40] Using higher pressures for FTS reaction is for now challenging in the *gas cell* TEM holder, and could also lead to difficulties in the image acquisition and capillary line plugging due to the formation of waxes. From a very qualitative point of view, we can observe the signals seem to stabilize faster in the case of Co on silica catalyst as compared to the Co on alumina catalyst, as the reduction of the particles is quite finished for the first catalyst at the beginning of the FT reaction, while the second one continues the reduction process under syngas leading thus to a progressive increase of the catalytic activity. This hypothesis is entirely

supported by the results obtained using TEM, during the reduction step and FT reaction, as well as by the evolution of the catalytic performances at the beginning of the FT reaction.

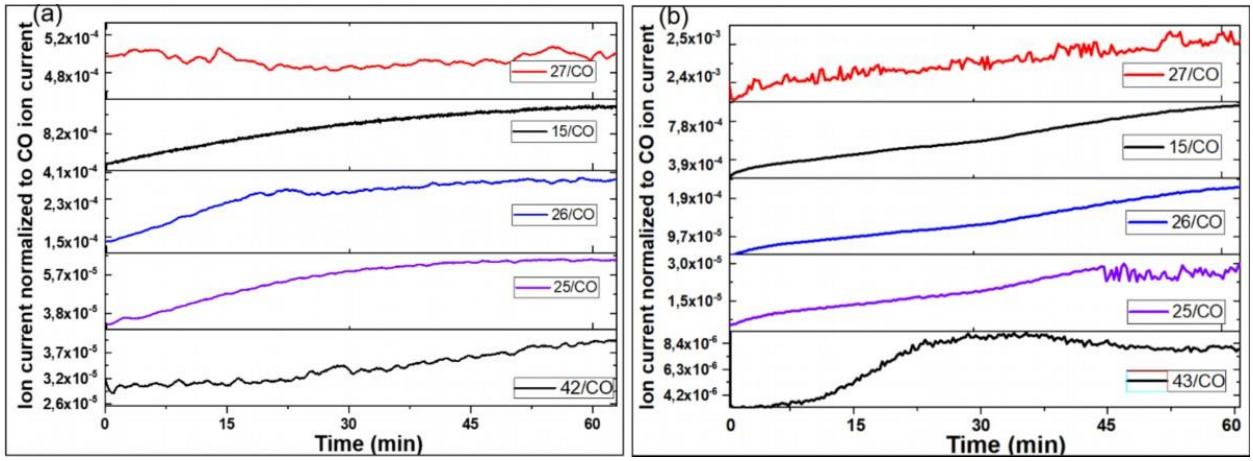


**Figure 6.** Ion current of the main gas products analysed by mass spectrometry during the Co-Pt/$SiO_2$ (a) and Co-Pt/$Al_2O_3$ (b) catalysts exposure to syngas ($H_2$/CO=2, 220 °C, 101.3 kPa).

## Conclusions

Using *in situ* TEM, we have provided direct insight on the structural and morphological changes of cobalt-based catalysts during the reduction step in relevant industrial activation conditions (101.3 kPa of $H_2$ at 430 °C) and their subsequent use for Fischer-Tropsch synthesis (101.3 kPa of $H_2$/CO=2 at 220 °C). We have firstly identified the morphological changes that do occur on individual nanoparticles and aggregates during the activation step using an industrial-like $Co_3O_4$-Pt/$Al_2O_3$-$SiO_2$ catalyst; simultaneously, we have evidenced the presence of water molecules in the reaction medium, here the environmental gas TEM cell, which can be considered as a good indicator of the reduction process in the cell. This corresponds to the loss of the cobalt aggregates porous structure, to particles aggregate fragmentation and to an apparent particles surface decrease as a result of the oxygen removal and particles densification. Similar characteristic reduction phenomena were observed on both $Co_3O_4$-Pt/$SiO_2$ and $Co_3O_4$-Pt/γ-$Al_2O_3$ catalysts. However, a lower starting temperature for the reduction process was evidenced for the silica support, which could imply an easier reduction of the $Co_3O_4$-Pt/$SiO_2$ catalyst compared to $Co_3O_4$-Pt/γ-$Al_2O_3$, in agreement with the evolution of the catalytic activity at the beginning of the FT process. After activation, both $Co_3O_4$-Pt/$SiO_2$ and $Co_3O_4$-Pt/γ-$Al_2O_3$ catalysts were exposed to syngas at

atmospheric pressure. The catalysts morphology was stable during the relatively short time on stream (1 h), however, a slight increase in particles size was observed. Using a residual mass spectrometry gas analysis connected to the exhaust line of the *in situ* TEM holder, we have detected the presence of mainly methane and $C_2$-$C_{4+}$ products during the catalyst operation.

From a material perspective, this in-situ analysis allowed us to directly asses the main morphological changes which are at the origin of the decrease of the performances of such catalysts in terms of selectivity or activity. Also, the obtained results clearly demonstrate the fact that the determination of the initial microstructure of the catalyst, before reduction, is not sufficient for understanding the catalytic performances of the catalyst which may considerably change during this activation step. Related to the role of the support, the comparison between the evolutions of the catalysts supported on alumina and on silica suggests that one the most valuable ways allowing to optimize the catalytic properties would be the synthesis of supports developing intermediate interactions with the particles, either by adding doping agents or by grafting silica islands on alumina.

This study highlights also the benefit of the *in situ* and *operando* environmental electron microscopy, when performed in relevant conditions for the studied processes, for the direct analysis of the structural evolution of the catalysts at the level of an individual particle. In the particular case of the catalytic system studied in this work, to better understand the influence of the particle size, type of support and platinum promotion on the syngas conversion and selectivity, further improvements will be conducted, in particular regarding the detection of the small amounts of reaction products with the mass spectrometer connected to the exhaust line of the TEM cell. This development paves the way for new in situ studies in this field and will allow investigating other phenomena, as for example the potential role of water vapours in the sintering or in the fragmentation process and their influence on the catalytic performances.

**Acknowledgments**

Dr. K. Dembélé thanks the Région Alsace and IFP Énergies Nouvelles for funding his PhD grant. Authors thank the French ANR (National Research Agency) under the 3DClean project 15-CE090009-01 for financial support.

## Bibliography


[1] E. Iglesia, *Appl. Catal. Gen.* **1997**, *161*, 59–78.
[2] H. Schulz, *Appl. Catal. Gen.* **1999**, *186*, 3–12.
[3] A. Y. Khodakov, W. Chu, P. Fongarland, *Chem Rev* **2007**, *107*, 1692–1744.
[4] D. Moodley, M. Claeys, E. van Steen, P. van Helden, D. Kistamurthy, K.-J. Weststrate, H. Niemantsverdriet, A. Saib, W. Erasmus, J. van de Loosdrecht, *Catal. Today* **2020**, *342*, 59–70.
[5] M. A. Vannice, *J. Catal.* **1975**, *37*, 462–473.
[6] B. C. Enger, A. Holmen, *Catal. Rev.* **2012**, *54*, 437–488.
[7] S. Shetty, R. A. van Santen, *Catal. Today* **2011**, *171*, 168–173.
[8] M. E. Dry, A. P. Steynberg, in *Stud. Surf. Sci. Catal.* (Eds.: A. Steynberg, M. Dry), Elsevier, **2004**, pp. 406–481.
[9] R. C. Reuel, C. H. Bartholomew, *J. Catal.* **1984**, *85*, 78–88.
[10] A. Y. Khodakov, *Catal. Today* **2009**, *144*, 251–257.
[11] Ø. Borg, P. D. C. Dietzel, A. I. Spjelkavik, E. Z. Tveten, J. C. Walmsley, S. Diplas, S. Eri, A. Holmen, E. Rytter, *J. Catal.* **2008**, *259*, 161–164.
[12] P. Munnik, P. E. de Jongh, K. P. de Jong, *J. Am. Chem. Soc.* **2014**, *136*, 7333–7340.
[13] A. P. Petersen, M. Claeys, P. J. Kooyman, E. van Steen, *Catalysts* **2019**, *9*, 794.
[14] F. Morales, B. M. Weckhuysen, *Catalysis* **2006**, 1–40.
[15] G. Jacobs, Y. Ji, B. H. Davis, D. Cronauer, A. J. Kropf, C. L. Marshall, *Appl. Catal. Gen.* **2007**, *333*, 177–191.
[16] M. Loewert, M.-A. Serrer, T. Carambia, M. Stehle, A. Zimina, K. F. Kalz, H. Lichtenberg, E. Saraçi, P. Pfeifer, J.-D. Grunwaldt, *React. Chem. Eng.* **2020**, *5*, 1071–1082.
[17] M. K. Rayner, D. G. Billing, N. J. Coville, *Acta Crystallogr. Sect. B* **2014**, *70*, 498–509.
[18] M. L. Taheri, E. A. Stach, I. Arslan, P. A. Crozier, B. C. Kabius, T. LaGrange, A. M. Minor, S. Takeda, M. Tanase, J. B. Wagner, R. Sharma, *Ultramicroscopy* **2016**, *170*, 86–95.
[19] M. Plodinec, H. C. Nerl, R. Farra, M. G. Willinger, E. Stotz, R. Schlögl, T. Lunkenbein, *Microsc. Microanal.* **2020**, 1–9.
[20] F. (Feng) Tao, P. A. Crozier, *Chem. Rev.* **2016**, *116*, 3487–3539.
[21] N. Fischer, M. Claeys, *J. Phys. Appl. Phys.* **2020**, DOI 10.1088/1361-6463/ab761c.
[22] I. K. van Ravenhorst, R. G. Geitenbeek, M. J. van der Eerden, J. Tijn van Omme, H. H. Peréz Garza, F. Meirer, A. Meijerink, B. M. Weckhuysen, *ChemCatChem* **2019**, *11*, 5505–5512.
[23] E. Prestat, M. A. Kulzick, P. J. Dietrich, Mr. M. Smith, Mr. E.-P. Tien, M. G. Burke, S. J. Haigh, N. J. Zaluzec, *ChemPhysChem* **2017**, *18*, 2151–2156.
[24] M. R. Ward, E. D. Boyes, P. L. Gai, *ChemCatChem* **2013**, *5*, 2655–2661.
[25] T. Paryjczak, J. Rynkowski, S. Karski, *J. Chromatogr. A* **1980**, *188*, 254–256.
[26] R. Dehghan, T. W. Hansen, J. B. Wagner, A. Holmen, E. Rytter, Ø. Borg, J. C. Walmsley, *Catal. Lett.* **2011**, *141*, 754.
[27] G. M. Bremmer, E. Zacharaki, A. O. Sjåstad, V. Navarro, J. W. M. Frenken, P. J. Kooyman, *Faraday Discuss.* **2017**, *197*, 337–351.
[28] S. B. Vendelbo, C. F. Elkjær, H. Falsig, I. Puspitasari, P. Dona, L. Mele, B. Morana, B. J. Nelissen, R. van Rijn, J. F. Creemer, P. J. Kooyman, S. Helveg, *Nat. Mater.* **2014**, *13*, 884–890.
[29] K. Dembele, M. Bahri, G. Melinte, C. Hirlimann, A. Berliet, S. Maury, A.-S. Gay, O. Ersen, *Chem. Cat. Chem.* **2018**, *10*, 3924-3924.

[30] Protochips, “Atmosphere,” can be found under http://www.protochips.com/products/atmosphere/, **2020**.
[31] J. P. den Breejen, P. B. Radstake, G. L. Bezemer, J. H. Bitter, V. Frøseth, A. Holmen, K. P. de Jong, *J. Am. Chem. Soc.* **2009**, *131*, 7197–7203.
[32] D. Song, J. Li, *J. Mol. Catal. Chem.* **2006**, *247*, 206–212.
[33] C. E. Kliewer, S. L. Soled, G. Kiss, *Catal. Today* **2019**, *323*, 233–256.
[34] S. Humbert, G. Desjouis, T. Bizien, L. Lemaitre, A. L. Taleb, C. Dalverny, L. Sorbier, A. S. Gay, *J. Catal.* **2018**, *366*, 202–212.
[35] G. Jacobs, T. K. Das, Y. Zhang, J. Li, G. Racoillet, B. H. Davis, *Appl. Catal. Gen.* **2002**, *233*, 263–281.
[36] L. Braconnier, E. Landrivon, I. Clémençon, C. Legens, F. Diehl, Y. Schuurman, *Catal. Today* **2013**, *215*, 18–23.
[37] A. M. Saib, D. J. Moodley, I. M. Ciobîcă, M. M. Hauman, B. H. Sigwebela, C. J. Weststrate, J. W. Niemantsverdriet, J. van de Loosdrecht, *Catal. Today* **2010**, *154*, 271–282.
[38] D. Kistamurthy, A. M. Saib, D. J. Moodley, J. W. Niemantsverdriet, C. J. Weststrate, *J. Catal.* **2015**, *328*, 123–129.
[39] A. Barbier, A. Tuel, I. Arcon, A. Kodre, G. A. Martin, *J. Catal.* **2001**, *200*, 106–116.
[40] J. Yang, W. Ma, D. Chen, A. Holmen, B. H. Davis, *Appl. Catal. Gen.* **2014**, *470*, 250–260.

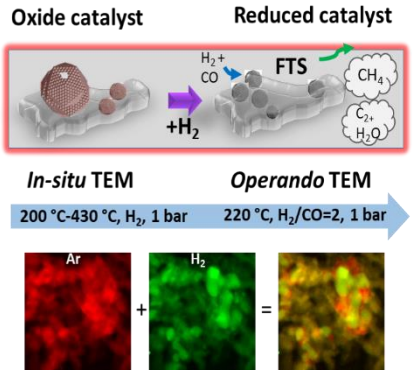


**Activate them and watch them work**! The behavior of cobalt nanocatalysts was monitored by coupling *in situ* TEM and mass spectrometry during the reduction step and Fischer-Tropsch reaction. Their evolution was correlated to structural processes such as particle fragmentation, migration and coalescence. An easier reduction of silica-supported catalyst as compared to alumina-supported one was evidenced. The results display the formation of methane and $C_2$-$C_{4+}$ products during reaction at 1 bar, with a catalytic behavior depending on the type of support.